JOURNAL OF GEOPHYSICAL RESEARCH, VOL. 102, NO. D17, PAGES 21,221–21,237, SEPTEMBER 20, 1997

Tropospheric chemical ozone tendencies in CO-CH_4-NO_y-H_2O system: Their sensitivity to variations in environmental parameters and their application to a global chemistry transport model study

A. Klonecki

Atmospheric and Oceanic Sciences Program, Princeton University, Princeton, New Jersey

H. Levy II

Geophysical Fluid Dynamics Laboratory/NOAA, Princeton, New Jersey

Abstract. A photochemical box model with CO-CH_4-NO_y-H_2O chemistry is used to calculate the diurnally averaged net photochemical rate of change of ozone (hereinafter called the chemical ozone tendency) in the troposphere for different values of parameters: NO_x and ozone concentration, temperature, humidity, CO concentration, and surface albedo. To understand the dependency of the chemical ozone tendency on the input parameters, a detailed sensitivity study is performed. Subsequently, the expected variations of the ozone tendencies with altitude, latitude, and season are analyzed. The magnitude of the tendency decreases rapidly with height mostly as a result of lower absolute humidity and temperature. In the upper troposphere (at 190 mbar) the maximum tendencies are below 2 parts per billion by volume/day. Lower temperature and specific humidity cause a shift of the value of NO_x at which the ozone production balances the destruction of ozone (balance point) to lower NO_x values; these two parameters are also, to a large extent, responsible for lower magnitudes of the tendency at higher latitudes and in winter. In the upper troposphere we find that the net tendency is at least as sensitive to variations in H_2O concentration as to NO_x. This suggests a possible synergism between direct NO_x pollution by aircraft and the indirect modification of H_2O by climate change. In the second part of the paper the box model calculated rates are used as ozone's chemical tendency terms during a simulation conducted with the three-dimensional global chemistry transport model (GCTM). The box model is used to calculate the tendencies as a function of NO_x and ozone at all tropospheric levels of the GCTM, at nine latitudes and for four seasons using zonally and monthly averaged data: water vapor and temperature from observations and model CO. These tables together with the NO_x fields obtained in an earlier GCTM simulation are used in the GCTM simulation of O_3 if nonmethane hydrocarbon levels are low. The global monthly averaged chemical ozone tendency fields saved during the simulation are presented and analyzed for the present-day and preindustrial conditions. The chemical tendency fields show a strong correlation with the NO_x fields. In contrast with the lower and middle troposphere where the tendencies are negative in remote regions over the oceans, in the upper troposphere, where NO_x is generally greater than 50 parts per trillion by volume and the balance point is low, the tendencies are generally small but positive. The GCTM simulations of the preindustrial ozone show that in the upper troposphere the present-day ozone tendencies are greater than the simulated preindustrial tendencies. In the boundary layer and in the midtroposphere the present-day tendencies are greater near anthropogenic NO_x sources and smaller (generally more negative), due to higher ozone levels, in regions not affected by these sources.

1. Introduction

Ozone is a tracer that has a significant influence on the chemical and radiative properties of the lower atmosphere. It is largely responsible for the oxidizing capability of the troposphere and it determines the lifetimes of many of the species found there. Ozone reacts directly with a number of trace gases, but its role as an oxidizing agent is greatly enhanced because of its importance in the production of tropospheric hydroxyl radicals (OH) [*Levy*, 1971]:

$$O_3 + h\nu \rightarrow O(^1D) + O_2 \quad \text{(J1)}$$

$$O(^1D) + H_2O \rightarrow 2\,OH \quad \text{(R4)}$$

Copyright 1997 by the American Geophysical Union.

Paper number 97JD01805.
0148-0227/97/97JD-01805$09.00

Hydroxyl radicals are extremely reactive and are responsible for the oxidation of many of the trace gases found in the troposphere including species such as CO and CH_4.

Tropospheric ozone is also an important greenhouse gas. Model studies show that the increase in tropospheric ozone has contributed about 0.5 W m^{-2} to the radiative forcing. This contribution amounts to about 20% of the 2.4 W m^{-2} attributed to the increase of all of the well-mixed gases [*Hauglustaine et al.*, 1994; *World Meteorological Organization*, 1994]. Another example of the importance of tropospheric ozone as a greenhouse gas has been given by *Ramanathan and Dickinson* [1979]. They showed that even though there is much less ozone in the troposphere than in the stratosphere a uniform percentage decrease of ozone in the troposphere would have a similar impact on the greenhouse effect as the change caused by the same uniform percentage decrease in stratospheric ozone. This fact can be explained by noticing that ozone absorbs long wave radiation more efficiently at higher pressures, because the opacity of the 9.6 μm absorption band increases with pressure.

Ozone can also, if present at the surface in large concentrations, be detrimental to human health and can cause plant damage [*National Research Council*, 1991; *Heck et al.*, 1982; *Skarby and Sellden*, 1984].

Tropospheric ozone can either be transported from the stratosphere, where its mixing ratio is much higher, or it can be produced through a series of photochemical reactions in the troposphere. *Junge* [1962] suggested that the concentration of tropospheric ozone is determined by transport of ozone from the stratosphere and destruction at the ground. This theory was first questioned by *Chameides and Walker* [1973] and *Crutzen* [1974]. They argued that photochemistry in the troposphere is responsible for the seasonal and daily variations in ozone density. A number of studies have been conducted since then to investigate the two sources [e.g., *Fabian*, 1974; *Chatfield and Harrison*, 1976; *Fishman et al.*, 1979; *Liu et al.*, 1980; *Mahlman et al.*, 1980], and it is now generally believed that both transport from the stratosphere and photochemical reactions in the troposphere can have an important impact on ozone concentrations in the troposphere [e.g., *Levy et al.*, 1985; *Follows and Austin*, 1992; *Jacob et al.*, 1992; *Roelofs and Lelieveld*, 1995; *Kasibhatla et al.*, 1996; *Mauzerall et al.*, 1996; *Levy et al.*, 1997]. However, there is still disagreement about the relative importance of these two sources, mainly because of the difficulties in estimating the contribution from chemical production. Ozone chemistry in the troposphere is very sensitive to the concentrations of ozone precursors (e.g., NO_x, H_2O, CO, and hydrocarbons) whose distributions are highly variable and not well known.

To estimate how much ozone is produced or destroyed in the troposphere, researchers use photochemical models. In these models a certain reaction mechanism is assumed, reaction rates for the specified conditions are calculated based on the measured rate constants, and the system of equations is integrated in time. The photochemical models have a number of limitations that have been described briefly by *Chameides et al.* [1987]. There are uncertainties in the reaction rates and there are also uncertainties in the assumed reaction mechanisms, especially when nonmethane hydrocarbons (NMHC) are included. If NMHC are to be modeled, mechanisms have to be condensed and surrogate species have to be introduced to substitute for whole classes of organic compounds, because it would not be computationally feasible to model hundreds of organic species present in the troposphere. Despite these limitations, chemical models can still yield useful and reasonably accurate results as confirmed by studies in which model simulations are compared against field measurements [e.g., *Lurmann et al.*, 1984; *Chameides et al.*, 1987; *Trainer et al.*, 1991; *Ridley et al.*, 1992; *Davis et al.*, 1996; *Jacob et al.*, 1996]. Models can also provide qualitative information about various dependencies that would otherwise be difficult to extract from the nonlinear systems, and they can give estimates of concentration of species that are difficult to measure.

Numerous investigators used photochemical models to look at production of ozone and ozone precursors. Important insight can be gained by using relatively simple box models or one-dimensional (1-D) models. *Levy* [1971] used a steady state photochemical box model to calculate concentrations of hydroxyl, hydroperoxyl, and methylperoxyl radicals. *Chameides and Walker* [1973] and *Crutzen* [1974] used similar models to argue that tropospheric ozone has a large source in the troposphere and that chemical processes determine ozone concentrations in the troposphere. Some investigators conducted sensitivity studies of how concentrations of ozone precursors influence net ozone production. The effect of changes in NO_x concentration has been studied by, for example, *Fishman and Crutzen* [1977], and *Chameides et al.* [1987]. *Trainer et al.* [1987] used a 1-D model to study the effect of natural and anthropogenic hydrocarbons on hydroxyl and peroxy radicals, and *Lurmann et al.* [1984] looked at the effect of natural hydrocarbons on ozone concentrations. *Chameides et al.* [1987] presented some sensitivity studies to show how ozone production would change if concentrations of H_2O, CO, NO, and O_3 were doubled. This calculation is done, however, for a small number of cases. In the first part of this paper (section 3) we present a detailed theoretical sensitivity study of the net chemical ozone tendency (difference between ozone production and destruction) in a simple CO-CH_4-NO_y-H_2O system. For this system with no nonmethane hydrocarbons we analyze the effect of the variations in the important input parameters: water vapor, temperature, ozone, CO, and amount of available solar flux for a range of NO_x mixing ratios. We extend this range beyond clean conditions (also for high NO_x) still neglecting nonmethane hydrocarbons to show the general trends in the behavior of the tendencies under such conditions. The additional effect of NMHC is discussed. We also analyze the variations in the chemical ozone tendency and the balance point with height, latitude, and season. The possible anthropogenic changes in the tendencies are discussed. In the second part of the paper (section 4) we present and discuss the simulated global chemical ozone tendency fields. They were calculated with the 3-D global chemistry transport model (GCTM) in which the instantaneous chemical ozone tendency terms at each time step were obtained from tables calculated with the box model with no NMHC. Recognizing the importance of NMHCs in ozone chemistry, the CO/CH_4 tendencies were used only in regions where the concentrations of NMHC are diagnosed to be low.

2. Description of the Photochemical Box Model

For both the theoretical sensitivity study and the GCTM application we use a zero-dimensional model employing CO/CH_4 chemistry to obtain the diurnally averaged chemical ozone tendency. The tendencies are calculated for specified mixing ratios of ozone and NOX (defined here as NO+ NO_2+

NO_3+ 2*N_2O_5) which are held constant throughout each integration. An alternative approach in which ozone mixing ratios are allowed to vary diurnally will also be presented later in the paper. The calculated tendencies are the diurnal averages of the sum of all the production rates of ozone minus all the destruction rates. The system of rate equations was integrated diurnally in time until the daily averaged chemical ozone tendency (given in parts per billion by volume (ppbv)/day) changed by less than 1% from day to day. The minimum time of integration for each case is 5 days. In the chemical model there is no explicit transport of species into and out of the box, although the fact that ozone concentration is held constant is a form of implicit transport. Whenever ozone is being produced, it can be assumed that the excess is transported out of the box or is deposited, and when it is destroyed, it is transported into the box. Other than this implicit transport, all transformations within the box happen as a result of chemical or photochemical reactions. The CO-CH_4 mechanism consists of 47 reactions given in Table 1. Rates of the photodissociation reactions are calculated with a radiative transfer model [*Perliski*, 1992; *Meier et al.*, 1982] that includes the effect of ground albedo and multiple Rayleigh scattering. Photodissociation rates were calculated for clear sky conditions for a specified month, latitude, albedo, and 11 zenith angles. The radiative transfer model takes as input observed temperature profiles [*Barnett and Corney*, 1985] and a merged ozone data set [*Orris*, 1997; *Logan*, 1985; *Komhyr et al.*, 1989; *Spivakovsky et al.*, 1990; *Keating et al.*, 1990]. The rates of the remaining reactions were calculated using the recommended values from *DeMore et al.* [1994]. We did not include primary sources of NO_x radicals other than H_2O. Species such as acetone (*Jacob et al.*, 1996, L. Jaeglé, personal communication, 1997) and peroxides can increase the HO_x concentration especially in the upper troposphere where concentration of water is small (L. Jaeglé, personal communication). The heterogeneous reactions were also not included; their role is discussed in section 3.4.3.

The CO/CH_4 mechanism has 22 species, seven of which are held at constant concentration: CH_4, H_2, O_2, CO, H_2O, O_3, and HNO_3. The first three represent the well-mixed species. The mixing ratio of methane was taken to be 1.7 ppm in the northern hemisphere and 1.6 in the southern hemisphere. The hydrogen mixing ratio was assumed to be 0.5 ppm. The CO data were taken from a GCTM simulation [*Kasibhatla et al.*, 1996], and water vapor and tropospheric temperatures were taken from observations [*Oort*, 1983]. Both CO and water vapor data sets were zonally and monthly averaged. The ozone mixing ratio is held constant for the reason given above. HNO_3 is held at a constant mixing ratio because its two main sinks, deposition and wet removal, are not included in the model. Our analysis finds that nitric acid at concentrations observed in the troposphere does not affect the chemical ozone tendency in a significant way.

The species with variable concentration are NO, NO_2, NO_3, N_2O_5, HNO_2, HNO_4, OH, HO_2, H_2O_2, CH_3O_2, CH_3OOH, H_2CO, CH_3O, $O(^1D)$, and $O(^3P)$. As mentioned above, the sum of the concentrations of the first four species is constant, but the partitioning between these species changes every time step. Since concentrations of NO_3 and N_2O_5 are very small during daytime when most of ozone is produced or destroyed, it will be assumed that this sum of the four nitrogen oxides is almost equivalent to NO_x ($NO+NO_2$). In the remainder of this paper all the results that are really a function of NOX (since

Table 1. Reactions Used in the Box Model

	Reaction
	Photodissociation Reactions
(J1)	$O_3+h\nu \rightarrow O_2+O(^1D)$
(J2)	$O_3+h\nu \rightarrow O_2+O(^3P)$
(J3)	$NO_2+h\nu \rightarrow NO+O(^3P)$
(J4)	$H_2O_2+h\nu \rightarrow 2OH$
(J5)	$HNO_3+h\nu \rightarrow OH+NO_2$
(J6)	$NO_3+h\nu \rightarrow 0.92*(NO_2+O(^3P))$ $+0.08*(NO+O_2)$
(J7)	$N_2O_5+h\nu \rightarrow NO_3+NO_2$
(J8)	$HONO+h\nu \rightarrow OH+NO$
(J9)	$HO_2NO_2+h\nu \rightarrow HO_2+NO_2$
(J10)	$HCHO+h\nu+(2O_2) \rightarrow 2HO_2+CO$
(J11)	$HCHO+h\nu \rightarrow CO+H_2$
(J12)	$CH_3OOH+h\nu \rightarrow CH_3O+OH$
	Nonphotodissociation Reactions
(R1)	$O(^3P)+O_2+M \rightarrow O_3+M$
(R2)	$O(^3P)+NO_2 \rightarrow O_2+NO$
(R3)	$O(^1D)+M \rightarrow O(^3P)+M$
(R4)	$O(^1D)+H_2O \rightarrow 2OH$
(R5)	$O(^1D)+CH_4 \rightarrow CH_3O_2+OH$
(R6)	$O(^1D)+H_2 \rightarrow HO_2+OH$
(R7)	$O_3+OH \rightarrow HO_2+O_2$
(R8)	$O_3+HO_2 \rightarrow 2O_2+OH$
(R9)	$OH+HO_2 \rightarrow H_2O+O_2$
(R10)	$HO_2+HO_2 \rightarrow H_2O_2+O_2$ $HO_2+HO_2+M \rightarrow H_2O_2+O_2+M$
(R11)	$OH+H_2O_2 \rightarrow H_2O+HO_2$
(R12)	$H_2+OH \rightarrow HO_2+H_2O$
(R13)	$O_3+NO \rightarrow O_2+NO_2$
(R14)	$HO_2+NO \rightarrow OH+NO_2$
(R15)	$OH+NO_2+M \rightarrow HNO_3+M$
(R16)	$HNO_3+OH \rightarrow NO_3+H_2O$
(R17)	$NO_2+O_3 \rightarrow NO_3+O_2$
(R18)	$NO_3+NO \rightarrow 2NO_2$
(R19)	$NO_3+NO_3 \rightarrow 2NO_2+O_2$
(R20)	$NO_2+NO_3+M \rightarrow N_2O_5+M$
(R21)	N_2O_5 (T) $\rightarrow NO_3+NO_2$
(R22)	$OH+NO+M \rightarrow HONO+M$
(R23)	$HONO+OH \rightarrow H_2O+NO_2$
(R24)	$HO_2+NO_2+M \rightarrow HO_2NO_2+M$
(R25)	HO_2NO_2(T) $\rightarrow HO_2+NO_2$
(R26)	$HO_2NO_2+OH \rightarrow H_2O+O_2+NO_2$
(R27)	$OH+CO+(O_2) \rightarrow CO_2+HO_2$
(R28)	$OH+CH_4+(O_2) \rightarrow CH_3O_2+H_2O$
(R29)	$CH_3O_2+NO \rightarrow CH_3O+NO_2$
(R30)	$CH_3O_2+HO_2 \rightarrow CH_3OOH+O_2$
(R31)	$CH_3O_2+CH_3O_2 \rightarrow 0.33(2CH_3O+O_2)$ $+0.66(CH2O+CH3OH+O2)$
(R32)	$CH_3O+O_2 \rightarrow HCHO+HO_2$
(R33)	$HCHO+OH+(O_2) \rightarrow HO_2+CO+H_2O$
(R34)	$CH_3OOH+OH \rightarrow 0.7(CH_3O_2+H_2O)$ $+0.3(H_2CO+OH+H_2O)$
(R35)	$NO_3+H_2CO+(O_2) \rightarrow HNO_3+HO_2+CO$

NOX is what is held constant) will be presented as a function of NO_x. HNO_2 and HNO_4 are in equilibrium with NOX. HNO_4, the more important of these two compounds, is not a part of NOX because its concentration in the upper troposphere may be comparable to NO_x, and the assumption that NOX is approximately equal to NO_x could not be made. In this theoretical study, peroxyacetylnitrate (PAN) is not included in the mechanism because its effect on ozone is mostly through changes in NOX, which is held constant. In the second part of the paper (section 4), in the applications to the GCTM study, PAN chemistry is included in the calculation of the NO_x fields (PAN in the GCTM is discussed by *Moxim et al.* [1996]).

As will be shown later in the paper, variations in albedo affect the chemical ozone tendencies. In this paper clear-sky conditions are assumed and only variations in the surface albedo are analyzed. In order to capture these variations, four types of surfaces were specified: snow-free and snow covered land and frozen and ice-free ocean. The values for snow-free land were taken from *Climate: Long-Range Investigation, Mapping, and Prediction* [1981]. For the snow-covered surfaces the extent of snow coverage in the northern hemisphere and the value of the snow albedo for different months were estimated based on the study by *Groisman et al.* [1994]. For both snow-free and snow-covered land the values of the albedo were zonally averaged. For grid boxes over ice-free sea, reflectance, which was calculated with Fresnel's law, was used to approximate the surface albedo. For sea ice the albedo was taken to be 0.7 [*List,* 1984].

For all but the last three of the species with varying concentrations, concentration at time $t+\Delta t$ is evaluated based on concentration $C(t)$, production $P(t)$, and destruction $D(t)*C(t)$.

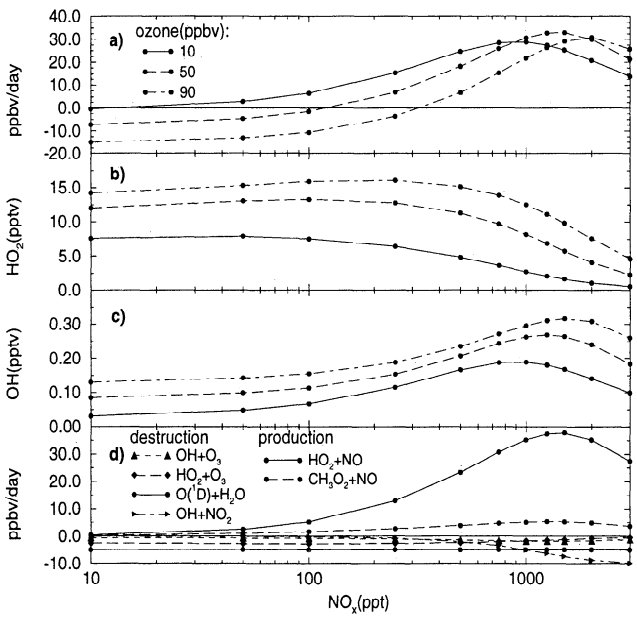

Figure 1. (a) Diurnally averaged chemical ozone tendency in units of ppbv/day as a function of NO_x. The three curves correspond to three different ozone concentrations: 10, 50, and 90 ppbv. The calculations were done for July conditions at 40°N and at the surface, (b) Diurnally averaged concentration of HO_2 in units of pptv, (c) Diurnally averaged concentration of OH in units of pptv, and (d) the main diurnally averaged production and destruction terms for the case from Figure 1a for 50 ppbv of O_3.

$P(t)$ and $D(t)$ are calculated for conditions at time t from the rate equations for the reactions that were included in the mechanism. The following differential equation is used to describe the rate of change of the concentration $C(t)$:

$$\frac{d}{dt}C(t) = P(t) - D(t)C(t)$$

To obtain the concentration at time $t+\Delta t$ it is assumed that $P(t)$ and $D(t)$ do not change during the time interval Δt. The following solution was used:

$$C(t+\Delta t) = \left(C(t) - \frac{P(t)}{D(t)}\right)e^{-D(t)\times\Delta t} + \frac{P(t)}{D(t)}$$

with time step Δt=60 s. Decreasing the time step did not introduce significant changes in the obtained results. CH_3O, $O(^1D)$, and $O(^3P)$, because of their short lifetimes, are assumed to reach steady state instantaneously, and their new concentrations are given by

$$C(t) = \frac{P(t)}{D(t)}$$

In order to analyze the effect of NMHC on the chemical ozone tendency, a set of results from the box model simulations that included the mechanism developed by *Gery et al.* [1989] is also presented in this paper.

3. Analysis

3.1. Chemical Ozone Tendency Versus Mixing Ratios of NO_x and Ozone

The first relationship that is analyzed in this paper is the well-known dependence of the chemical ozone tendency on NO_x mixing ratios. The curve shown in Figure 1a shows the tendencies calculated for a range of NO_x and ozone values with the CO/CH_4 mechanism for summer at 40°N near the surface. In this figure, for each ozone mixing ratio, three NO_x regions can be distinguished: a region with low mixing ratios of NO_x, where the tendency is negative, a region with higher NO_x, where the tendency is positive and is growing quickly with NO_x, and a region of very high NO_x (here more than 1-2 ppbv) where the tendency decreases with NO_x. The reasons for such strong dependence of the chemical ozone tendency on NO_x are well understood and are summarized here.

At low NO_x concentrations, production of ozone is slow and it is destruction that dominates (Figure 1d). The reaction that is especially important for destruction of ozone is the (J1) photodissociation of ozone and (R4) which is also a source of HO_x radicals. One molecule of ozone is lost as a result, but since the produced HO_x radicals react with ozone through (R7) and (R8), more ozone is destroyed.

$$O_3 + OH \rightarrow HO_2 + O_2 \quad \text{(R7)}$$

$$O_3 + HO_2 \rightarrow OH + 2O_2 \quad \text{(R8)}$$

For higher NO_x concentrations, production of ozone increases and eventually, for high enough NO_x, production surpasses destruction and the tendency becomes positive. NO_x owes its importance in the ozone production process to the quick photodissociation of NO_2 in the troposphere. Photolysis of NO_2 results in the formation of an oxygen atom, which combines rapidly with an oxygen molecule to form ozone.

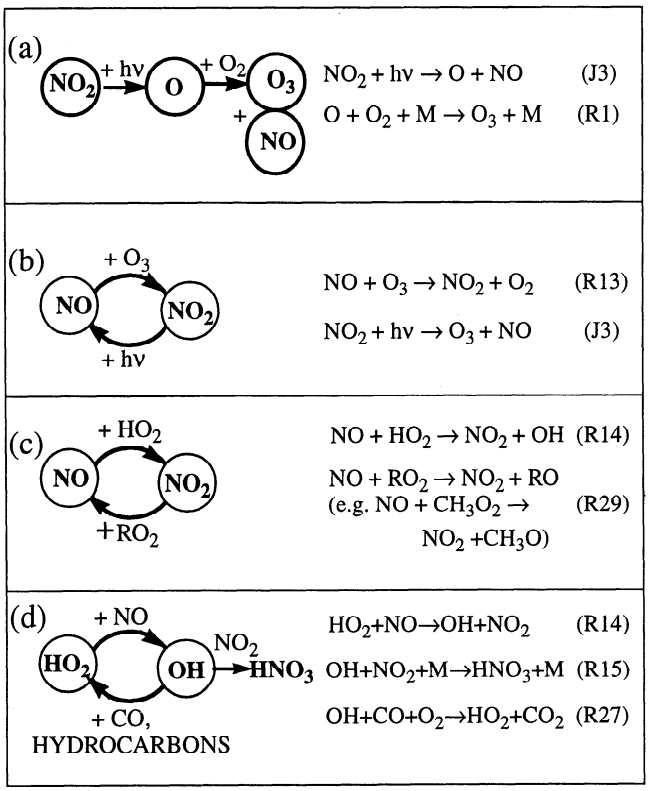

Figure 2. Schematic representation of reactions leading to ozone production and destruction.

The sequence of these two reactions, which are shown in Figure 2a, represents the dominant chemical source of ozone in the troposphere.

In order for production of ozone through the path depicted in Figure 2a to continue, NO has to be converted back to NO_2. The quickest reaction that oxidizes NO to NO_2 is the reaction with O_3, but since one ozone molecule is destroyed in this reaction, the net chemical ozone tendency of the cycle presented in Figure 2b is 0. In order to have net production, the rate of (J3) must be greater than the rate of (R13), or in other words, NO needs to be converted into NO_2 without first destroying ozone. Reactions with the peroxy radicals (Figure 2c) are responsible for such a conversion (R in RO_2 represents an organic group). Once NO is converted to NO_2, nitrogen dioxide photodissociates (provided solar radiation is available), and a molecule of ozone is produced, as shown in Figure 2a. Reactions between peroxy radicals and NO effectively determine the rate of production of ozone, and it is for this reason that the concentration of peroxy radicals is so crucial for the production of ozone. From the discussion above it is also apparent that NO_x acts as a catalyst and that the greater the concentration of NO_x, the quicker ozone production should be. Indeed, such an increase is observed for NO_x less than about 1 ppbv for the case presented in Figure 1a, but for values that are around 1 ppbv, the tendency starts to level off, and for even higher NO_x concentrations it actually decreases. The reason for this decrease becomes clear if the effect of added NO_x on OH radicals is analyzed. OH radicals are crucial for the formation of peroxy radicals, which are, as mentioned above, needed for ozone production. The cycling between hydrogen peroxy radical (HO_2) and hydroxyl radical (OH) for relatively high levels of NO_x is depicted in Figure 2d. As shown in Figure 1c, for NO_x less than about 1 ppbv in this case, concentration of OH radicals grows when more NO_x is added, because the rate of (R14) increases, and concentration of hydroxyl radicals grows at the expense of hydrogen peroxy radicals (the initial rise in HO_2 concentration with NO_x in Figure 1b is caused by methane oxidation cycle which, as NO_x increases, becomes a smaller sink and, for high enough NO_x, a source of HO_x). HO_2 is recreated mostly in the reactions between OH and CO, and between OH and hydrocarbons. With increasing mixing ratios of NO_x the reaction between NO_2 and OH in which nitric acid is produced gains importance. Since HNO_3 is not in equilibrium with NO_2 and OH, this reaction, for large mixing ratios of NO_x, represents an important sink for OH radicals and results in a significant depletion of HO_x. At high enough concentration of NO_x, adding more NO and NO_2 causes a greater percentage decrease in HO_2 than an increase in NO, and as a result the product of $[HO_2]$*[NO], and therefore the rate of (R14), begins to decrease. Similarly, the rate of the other reaction that converts NO into NO_2, the reaction between CH_3O_2 and NO, begins to slow down when NO_x reaches some threshold value, because the concentration of methoxy radical decreases rapidly. Since these two reactions determine the rate of ozone production (Figure 2c), the net chemical ozone tendency will also decrease as shown in Figure 1a.

Figure 1a also shows how the chemical ozone tendency depends on ozone. For mixing ratios of NO_x lower than about 1ppbv the tendency is higher for lower ozone. This relationship was expected since higher ozone leads to increased destruction, mostly through (J1) and (R4). Even though concentration of HO_2 radicals increases if more ozone is added (Figure 1b), rates of (R14) and (R29) (which as mentioned above are the rate-determining reactions for ozone production) are not necessarily greater, because less NO is available for conversion to NO_2 (the ratio of NO/NO_2 decreases significantly due to (R13)). A significant increase in destruction and not much change in production leads to the situation that is depicted in Figure 1a.

Another feature that is of interest is the shift in the position of the chemical ozone tendency maximum. For higher ozone mixing ratios, the maximum is at higher NO_x levels (Figure 1a). The reason for this shift can be attributed to the higher concentration of HO_x radicals (Figure 1b). Because there are more HO_2 and OH radicals, more NO_x is needed before (R15) begins to affect the production of ozone. The relative magnitudes of the maximum tendencies in Figure 1a depend on the relative magnitudes of the terms responsible for ozone production and destruction.

Figure 1a also shows that the balance point, or the value of NO_x for which the chemical ozone tendency is 0, is greater for higher ozone. Such a relationship was also expected since for higher ozone more NO_x is needed to counterbalance stronger destruction.

3.2. Chemical Ozone Tendency as a Function of Altitude: Sensitivity of the Tendency to Changes in Humidity and Temperature

Figure 3a shows the curves obtained for the same ozone mixing ratio of 50 ppbv but at three different pressures: 990 mbar (near the surface), 500 mbar (5.7 km), and 190 mbar (12.5 km). Appropriate values for temperature, humidity, and CO were taken for each of these surfaces, as described in section 2. The most striking differences between the curves are

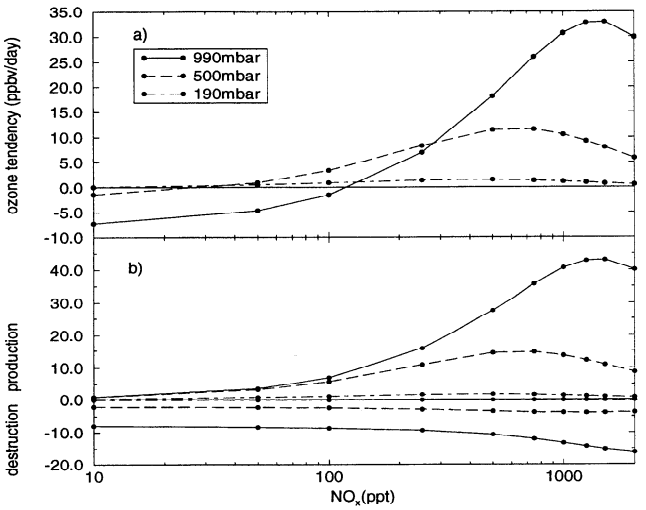

Figure 3. (a) Diurnally averaged chemical ozone tendency for 50 ppbv of ozone at three different pressure surfaces: 990, 500, and 190 mbar. Appropriate values for temperature, humidity, and CO were taken for each of the pressure surfaces as described in section 2. The calculations were done for July conditions at 40°N. (b) Approximation of diurnally averaged chemical production (positive values) and destruction (negative values) of ozone at the three pressure surfaces. Production was approximated as the sum of the rates of (R14) and (R29), and destruction as the sum of (R4), (R7), (R8), and (R15).

the sharp decreases in the magnitudes of the tendencies with increasing altitude and the rapid decrease in the NO_x balance point. The main reason for both of these differences is the quick decrease in the specific humidity (other HO_x sources such as acetone and convectively lifted peroxides were not included) and temperature with height. Figure 4, which shows the results of the ozone tendency calculations at 190 mbar for different temperatures and humidities, demonstrates this point. Raising temperature from 220 K to the surface value of 292 K (keeping water vapor mixing ratio the same) significantly increases the magnitude of the tendency for NO_x higher than about 50 parts per trillion by volume (pptv), and raising both temperature and humidity to the surface values raises the magnitude of the tendency (in units of ppbv/day) to values that are greater than levels obtained for the surface calculations (see Figure 1a). Therefore both lower humidity and lower temperature reduce the magnitude of the chemical ozone tendency at higher altitude. Lower number density at 190 mbar also plays a role, but it has the opposite effect. If it were only the number density that decreased, the chemical ozone tendency given in units of ppbv/day would be greater at lower pressure, mainly because the three-body reaction that is an important sink of HO_x radicals (R15), would be slower. In the troposphere the changes in photodissociation rates with height do have an impact on the tendencies but, for the assumed clear-sky conditions, this effect is much smaller than the one due to decreasing water vapor and temperature. In the troposphere the photolysis rates generally increase with altitude (although for some rates this trend can be reversed because of the temperature dependence of the quantum yields and cross sections and also due to Rayleigh scattering and surface albedo), and this effect slightly counteracts the decrease caused by lower water vapor concentration and temperature. For the case from Figure 3a the increase in photolysis rates alone between 990 and 190 mbar increases the ozone tendencies at 190 mbar by about 30%. Figure 3a shows that the mixing ratio of NO_x at which the chemical ozone tendency reaches a maximum decreases with altitude. At 190 mbar it is only about a half of what it is at the surface. Also the balance point shifts to much lower NO_x mixing ratios. These dependencies can be understood by analyzing the effects that water vapor concentration and temperature have on the ozone tendencies.

3.2.1. Effect of water vapor. With decreasing water vapor mixing ratio, fewer of the $O(^1D)$ radicals produced through ozone photodissociation react with H_2O to form HO_x radicals, and more react with an oxygen molecule to recreate ozone. As a result, the destruction of ozone decreases when humidity is lowered (Figure 5a). However, lower HO_x concentration leads

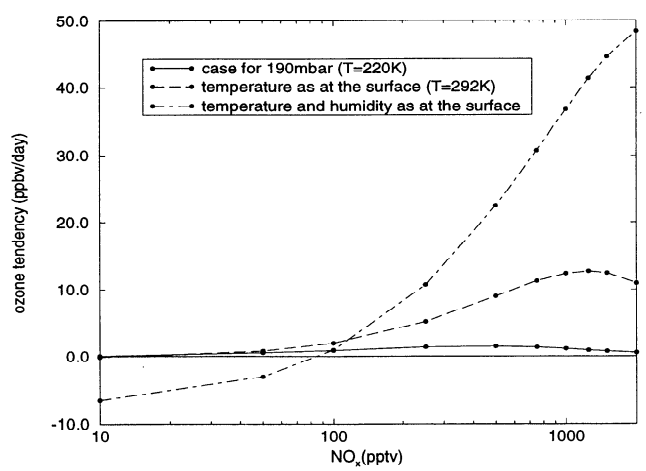

Figure 4. Diurnally averaged chemical ozone tendency at 190 mbar for 50 ppbv of ozone at 40°N and in July (solid line), diurnally averaged chemical ozone tendency at 190 mbar with temperature elevated to the surface value of 292 K (dashed line), and diurnally averaged chemical ozone tendency at 190 mbar with both temperature and mixing ratio of water elevated to the surface values (dot-dashed line).

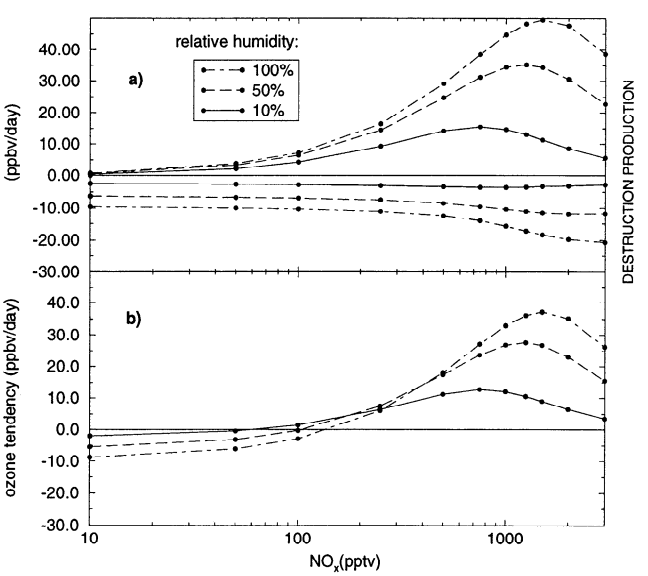

Figure 5. (a) Approximation of diurnally averaged chemical production (positive values) and destruction (negative values) of ozone at the surface at 40°N for July and for three different relative humidities: 100%, 50%, and 10%. Ozone concentration is 50 ppbv. Production and destruction defined as in Figure 3b. (b) Diurnally averaged chemical ozone tendency for 100%, 50%, and 10% relative humidities.

also to weaker production. Figure 5a shows that for the low NO_x values, the differences in destruction for the cases with different humidities are greater than the differences in production. For higher NO_x this relationship is reversed. Such changes in production and destruction explain the behavior of the chemical ozone tendency curves for decreasing humidity depicted in Figure 5b. In the low NO_x regime, the tendency increases when less water is present, and for NO_x higher than a certain value, the tendency decreases as a result of decreased production. Lower HO_x concentration for runs with lower humidity, just as in the case from section 3.1, is responsible for the shift of the peak of the maximum chemical ozone tendency to lower NO_x values. The balance point can also be seen to shift to the left because when humidity decreases, less NO_x is needed before production of ozone starts to balance weaker destruction.

Figure 5b suggests that changes in water vapor concentration can be as important for the chemical ozone tendency as variations in concentration of NO_x. Figure 5 depicts the surface case, but the strong effect of water vapor is especially pronounced in the upper troposphere. Figure 6 shows the tendencies at 190 mbar for two different temperatures: -52°C and -55°C, and for three different relative humidities: 10%, 30%, and 50%. Assuming that NO_x falls in the range of 50 to 500 pptv, it can be seen that changes in the water vapor concentration (caused by either changes in relative humidity or by changes in specific humidity resulting from a temperature change) can be as important for the tendency as changes in the NO_x mixing ratio arising, for example, from airplane emissions. Spatial variability in H_2O or changes in specific humidity arising from a systematic climate change can therefore significantly affect the chemical ozone tendency in the upper troposphere. In addition, the slopes are generally greater for the cases with higher water vapor concentration; therefore an increase in NO_x will result in a greater change in the ozone production if the humidity is high.

3.2.2. Effect of temperature. While changes in temperature affect two important parameters, water vapor concentration and the density of air, temperature alone can also have an important impact because reaction rate coefficients are temperature dependent. In this example, one simulation was run

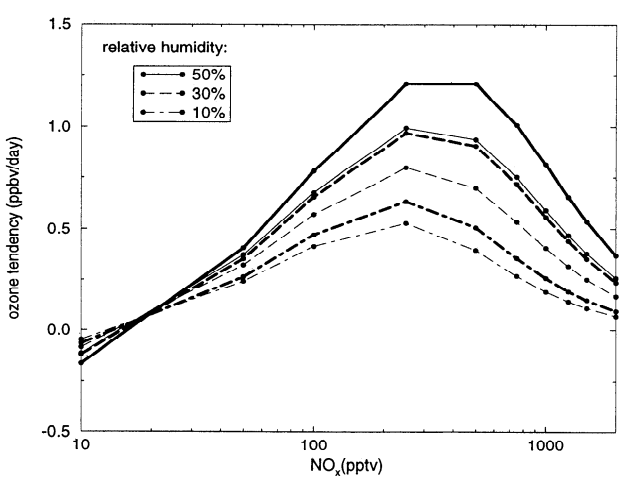

Figure 6. Diurnally averaged chemical ozone tendency at 190 mbar in July at 40°N for 100 ppbv of ozone for three different relative humidities: 50%, 30%, and 10%. The thick lines represent the ozone tendency curves calculated at -52°C; the thin lines represent the curves obtained at -55°C.

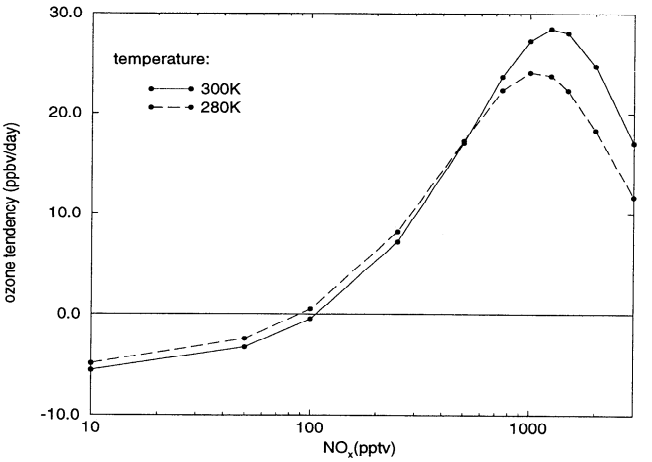

Figure 7. Diurnally averaged chemical ozone tendency at the surface in July at 40°N for 50 ppbv of ozone for two temperatures: 280°K and 300°K. For both cases the water vapor mixing ratio is the same, and it corresponds to about 30% relative humidity at 300°K and to about 100% at 280°K.

at 300 K and the other at 280 K. Mixing ratio of water vapor was kept constant (relative humidity increased from about 30% at 300 K to about 100% at 280 K) in order to isolate the effect of temperature (changes in density of air played only a minor role for a change of 20 K). To avoid unrealistic relative humidities, tendencies at temperatures below 280 K are not considered in this example. Figure 7 shows the general behavior of the tendencies at lower temperatures. Just as in Figure 4, the tendency is expected to be lower for high NO_x and slightly higher for low NO_x.

To understand the reason for such a dependence, one has to look at the reactions which have rates sensitive to temperature variations and which are important for ozone production or destruction. A number of reactions that control HO_x concentration meet these criteria; for example, the rate constant of (R28) decreases by almost 35% when temperature decreases from 300 K to 280 K. Changes in rates of (R10) and (R15) (both are HO_x sinks and are quicker at lower temperatures) are also important. Another reaction that is important is (R13) which is slower at colder temperatures. For much lower temperatures, such as the temperatures characteristic of the region near the tropopause, a mechanism that involves HNO_4 affects HO_x concentration and therefore the chemical ozone tendency. At low temperatures, HNO_4 is thermally stable, and reactions such as photodissociation and reaction with OH are the main loss pathways. For conditions that are especially favorable for HNO_4 formation, low temperatures and high concentrations of NO_2 and HO_2, HNO_4 can become a large fraction of total reactive nitrogen and the reaction with OH can become a significant sink for HO_x radicals:

$$HNO_4+OH \rightarrow H_2O+NO_2+O_2 \qquad \text{(R26)}$$

At higher temperatures, HNO_4 undergoes a rapid thermal decomposition and its influence is much smaller.

3.3. Chemical Ozone Tendency for Different Latitudes and Seasons

3.3.1. Latitudes. Figure 8a, which shows the daily averaged chemical ozone tendencies calculated at the equator, 20°N, 40°N, 60°N, and 80°N, clearly demonstrates the depen-

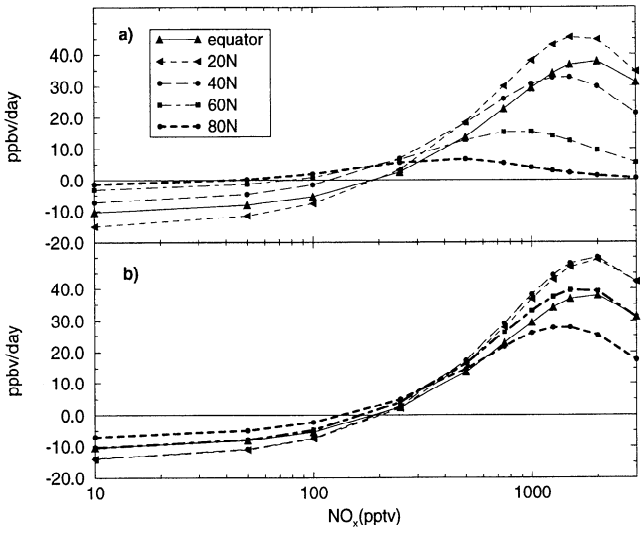

Figure 8. (a) Diurnally averaged chemical ozone tendency for 0°N, 20°N, 40°N, 60°N, and 80°N. The calculations were done for 50 ppbv of ozone for July and at 990 mbar. For each of the latitudes, zonally averaged values were assigned to all parameters as described in section 2. (b) Diurnally averaged chemical ozone tendency for 0°N, 20°N, 40°N, 60°N, and 80°N with all zonally averaged parameters (i.e., water vapor and CO concentration, temperature, albedo, ozone column) set equal to the corresponding values at the equator.

dence of the tendencies on latitude. At low NO_x the lowest tendencies can be observed at 20°N, and the highest can be observed at high latitudes (slowest destruction). For high NO_x the opposite dependence is observed, and the values at 20°N are more than an order of magnitude higher than at 80°N. Larger zenith angles are to a large extent responsible for the lower magnitudes of the tendency at high latitudes, but as expected, variations in the zonally averaged parameters such as humidity, temperature, and the ozone column (these parameters were assigned to zonally averaged values as described in section 2) also play a crucial role.

In order to see the effect of variations in the zenith angle alone, a separate set of calculations was done in which temperature, humidity, and the concentrations of all the species at all latitudes were set to be the same as at the equator. Also the ozone column, albedo, and temperature profiles used to calculated the J values were the same as the values used at the equator. Figure 8b, which depicts the results, shows that there are substantial differences between the two graphs. For example, the maximum tendency is now reached at 40°N (due to longer days) and not at 20°N, as shown in Figure 8a, and the tendency at 80°N is not much lower than the tendency at the equator. The differences between the two figures point to the importance of the values assigned to the zonally averaged parameters. Especially important are the differences in the ozone column and humidity. Figures 8a and 8b show that with increasing latitude the changes in the zonally averaged parameters can be responsible for a greater reduction of the magnitude of the daily averaged chemical ozone tendency than the reduction of the zenith angles alone. The tendencies at other tropospheric levels exhibit similar behavior.

3.3.2. Seasons. Figure 9 shows the results of calculations performed at 40°N for both winter and summer for the lower, middle, and upper troposphere. The magnitudes of the chemical tendencies can be more than 10 times smaller in winter, and the main reason for such a reduction is the combination of much larger zenith angles and shorter days. Much lower humidity and lower temperatures also play a significant role. Lower solar flux as well as lower humidity and temperature contribute to the shift of the maximum tendency and the balance point to lower NO_x mixing ratios in agreement with the analysis from section 3.2.

3.4. Sensitivity of the Chemical Ozone Tendency to Other Parameters Used in the Calculations

3.4.1. CO. To test the sensitivity of the ozone tendency to different CO levels, a case was run at the surface, 500 and 190 mbar with CO at 50, 100, and 200 ppbv. Figure 10 shows that for large NO_x the difference between the cases with different CO concentrations is large. Higher CO concentration causes quicker conversion of hydroxyl radicals to hydrogen peroxy radicals through (R27). This increase in HO_2 concentration is responsible for the increase in the rate of (R14), which, as mentioned in section 3.1, controls the rate of the ozone production. In the low NO_x regime where (R14) is less important, the difference between the cases with different CO mixing ratios (especially at the surface and 500 mbar) is much smaller.

For the calculations of the chemical ozone tendency that are depicted in Figure 10, concentration of CO was set to a constant value and was the same for all mixing ratios of NO_x. However, if either combustion of fossil fuels or biomass burning are the main sources of NO_x, then mixing ratio of CO is likely to increase with NO_x concentration. Figure 10 gives an estimate of the impact of scaling of the CO concentration to the NO_x level.

3.4.2. Surface albedo. To test the sensitivity of the calculated chemical ozone tendency to the surface albedo, the box model was run with photolysis rates calculated for two different albedos. One for a low surface albedo of 0.05, a value that represents, for example, the ocean at relatively small zenith angles, and the other set for a high value of 0.3, which can

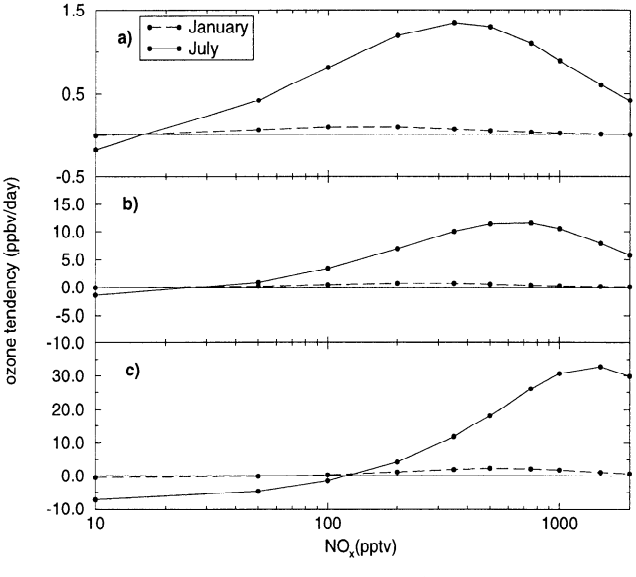

Figure 9. Diurnally averaged chemical ozone tendency in January and in July. The curves were obtained at 40°N for (a)100 ppbv at 190 mbar, and 50 ppbv of ozone at (b) 500 mbar, and (c) the surface.

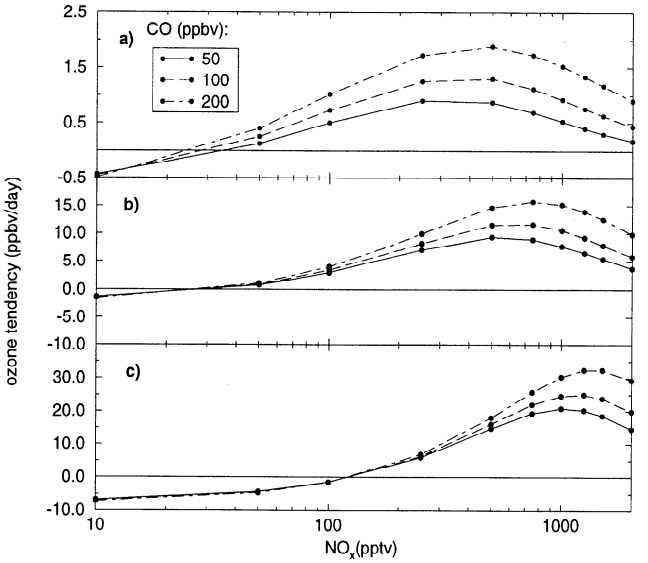

Figure 10. Diurnally averaged chemical ozone tendency at three pressure surfaces: (a) 190, (b) 500, and (c) 990 mbar for three CO mixing ratios: 50, 100, and 200 pbbv. The curves were obtained for conditions at 40°N in July; ozone mixing ratio is 150 ppbv at 190 mbar, and 50 ppbv at 500 mbar and 990 mbar.

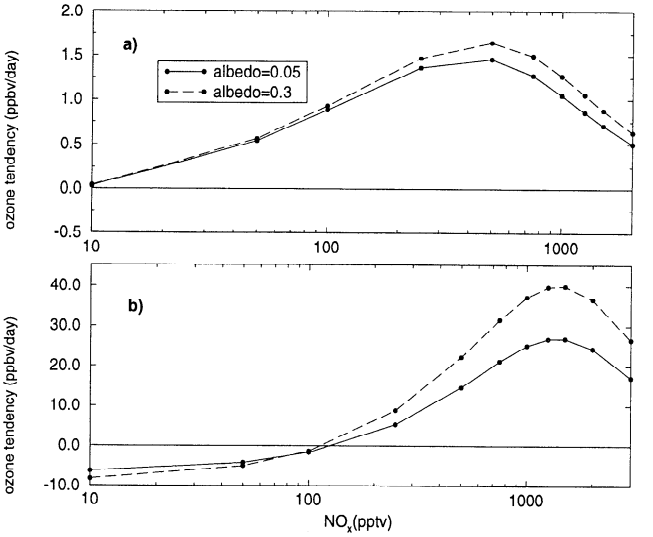

Figure 11. Diurnally averaged chemical ozone tendencies at (a) 190 and (b) 990 mbar for two values of surface albedo: 0.05 and 0.3. The calculations were done for conditions at 40°N in July and for 50 ppbv of ozone.

represent the albedo of sand. At the ground the differences are large and can reach up to 30% for small zenith angles. As expected, these differences get smaller with altitude because the path length for the reflected light increases. Figure 11 shows the effect of the different surface albedos on the chemical ozone tendencies at 990 and 190 mbar. At the ground the largest difference of about 15 ppbv/day, or about 30%, takes place for NO_x values of about 1.5 ppbv. For other NO_x levels, and especially at low NO_x, the difference is not as pronounced. At 190 mbar, where the effect of surface albedo is weaker, the relative differences are significantly smaller.

Variations in photolysis rates caused by changes in the ozone column or especially by the presence of clouds will cause similar effects. For example, at 40°N in summer, a 20% reduction of the ozone column (uniform throughout the atmosphere) resulted in the maximum chemical ozone tendency at the surface being about 10 ppbv/day higher (about 30%).

3.4.3. Heterogeneous removal of N_2O_5 and NO_3. Heterogeneous removal of N_2O_5 and NO_3 can have a direct effect on ozone concentration [*Dentener and Crutzen*, 1993] ($2O_3$ removed for each NO_3 lost and $3O_3$ removed for each N_2O_5), as well as an indirect effect caused by the decrease in the NO_x concentration. Since in this theoretical sensitivity study the concentration of nitrogen oxides is assumed to be constant, the indirect effect is not important. The direct effect, which can lower the ozone tendency under high NO_x conditions, is not included in the theoretical study but is accounted for in the GCTM ozone simulations discussed in section 4 [*Levy et al.*, 1997; H. Levy II, Tropospheric NO_x: Its sources and distribution, manuscript in preparation, 1997] (hereinafter referred to as Levy et al., manuscript in preparation, 1997).

3.5. Chemical Ozone Tendency With Variable Ozone

In all the calculations presented so far, ozone concentration was held constant throughout each integration (see section 2). This approach was adopted in order to be able to compute the tendency for a given ozone concentration (by definition, if the box model described in section 2 is integrated with changing ozone, no equilibrium is reached until the ozone concentration reaches a diurnal steady state and the tendency is essentially 0). To investigate the effect of this constraint on the calculated daily average ozone tendency, a case was run where ozone was allowed to change during the last 24 hours of the integration after the stability criterion described in section 2 had been reached. Figure 12 shows that the two cases do not differ significantly. The small differences that are present can be understood with the help of Figure 1a which shows how the chemical ozone tendency reacts to different levels of ozone. If the tendency is negative, ozone concentration will decrease in the scenario where ozone is allowed to

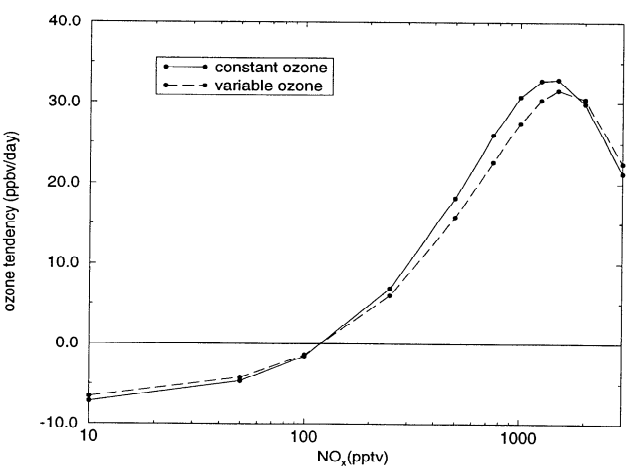

Figure 12. Diurnally averaged chemical ozone tendency for a case with constant ozone (solid line), and a case where ozone is allowed to change during the last day of the simulation after the stabilization criteria have already been met (dashed line). The calculations were performed at 40°N in July and for initial 50 ppbv mixing ratio of ozone.

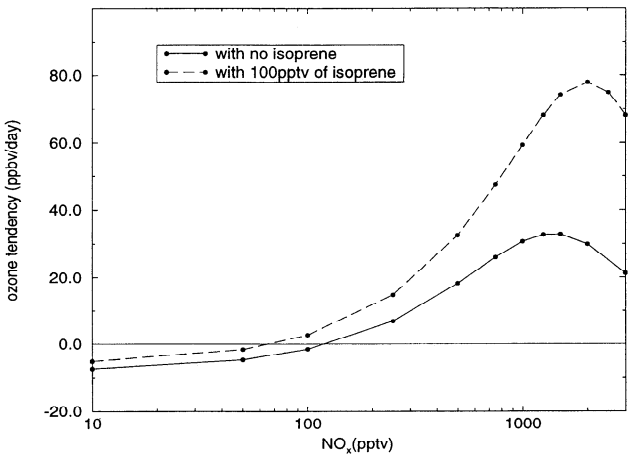

Figure 13. Diurnally averaged chemical ozone tendency with no isoprene (solid line) and with 100 pptv of isoprene (dashed line). The calculations were performed for conditions at the surface at 40°N in July and for 50 ppbv of ozone.

change, and ozone destruction will be slower. If the tendency is positive, the case with changing ozone will have a higher concentration of ozone, and for the case depicted in Figure 1a, for NO_x less than about 1.5 ppbv of NO_x, the tendency will be lower, and for NO_x higher than 1.5 ppbv, it will be higher. The greater the absolute value of the tendency, the greater the change in ozone in the case with variable ozone, and the greater is the difference between the two cases.

3.6. Chemical Ozone Tendency With NMHC

Figure 13 shows how the addition of NMHC can affect the chemical ozone tendency [see, e.g., *Liu et al.*, 1987]. It is assumed that isoprene is the only NMHC with a source, and its concentration is held at 100 pptv throughout the integration. Any other NMHC present is a by-product of isoprene oxidation. A condensed carbon bond mechanism (CB IV) mechanism developed by *Gery et al.* [1989] was added to the CO/CH_4 mechanism. Carbon bond mechanisms are based on the principle that similarly bonded carbon atoms can be treated as one surrogate species [*Whitten et al.*, 1980], so, for example, all single-bonded carbon atoms are treated as one species, no matter what molecule they are a part of. In Figure 13 it becomes immediately apparent that the chemical ozone tendencies, even for only 100 pptv of isoprene, are for NO_x greater than about 100 pptv much higher than they are for the CO/CH_4 only case and that the ozone tendency maximum is moved to higher NO_x values. Organic peroxy radicals (RO_2) formed during oxidation of NMHC are responsible for the higher production of ozone, because RO_2 radicals increase the conversion of NO to NO_2 (see Figure 2c). The shift in the ozone tendency maximum can be explained in a similar way as in section 3.1. If NMHCs are present, the concentration of HO_x radicals goes up, and (R15), which is a sink for radicals, does not become significant until higher values of NO_x. NMHCs also convert OH radicals into HO_2 and therefore slow down the rate of (R15). For much greater concentrations of NMHCs, the maximum chemical ozone tendency is at considerably higher NO_x values.

3.7. Sensitivity of the Calculated Chemical Ozone Tendencies to the Uncertainties in the Reaction Rate Constants

For this study rate constants for all nonphotodissociation reactions were taken from *DeMore et al.* [1994]. This publication lists parameters that can be used to estimate the uncertainties for the rate constants that correspond approximately to one standard deviation. It is further assumed that the uncertainty is smallest at 298 K, and that it increases for higher or lower temperatures. It is emphasized that due to the lack of sufficient data, the values of the uncertainties are not based on a statistical analysis but on subjective judgments of the authors [*DeMore et al.*, 1994]. We use these suggested values to estimate the possible error resulting from the uncertainties in the reaction rate constants of bimolecular reactions. Figure 14a shows the results for the reactions that introduce the greatest uncertainty to the calculated tendencies at 990 mbar when ozone is 30 ppbv and NO_x is 100 pptv. These results were obtained by running the box model with the rate of only one reaction changed at a time by the estimated uncertainty. It can be seen that uncertainty in the rate of (R14) has the greatest effect on the ozone tendency, in this case about 30%. For other conditions this effect will be different, because the relative significance of the reactions can change. At 190 mbar (Figure 14b) the uncertainties in the rate constants are generally larger because of the mentioned temperature dependence. The largest possible error at this pressure for 100 ppbv of ozone and 200 pptv of NO_x is introduced by (R27), and it is also about 30%. A thorough study by *Thompson and Stewart* [1991] employing a Monte Carlo technique shows that the uncertainty in the rate constants can introduce a standard devia-

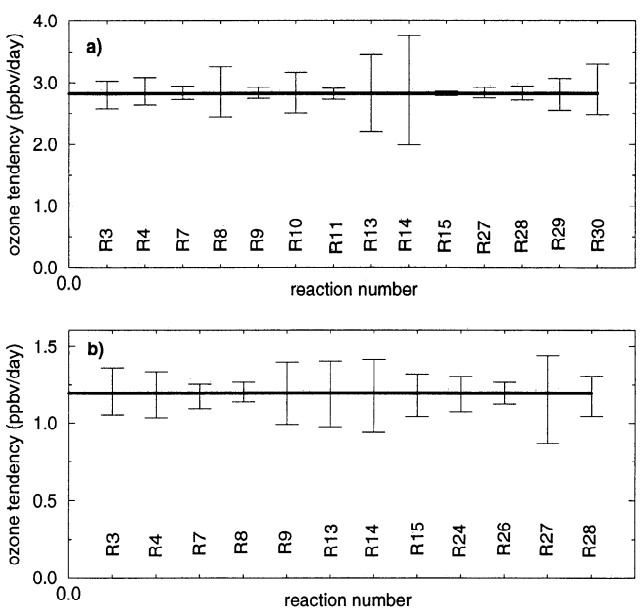

Figure 14. The uncertainties in the calculated chemical ozone tendencies resulting from the uncertainties in the reaction rate constants of a single reaction. The thick solid line represents the tendency with no error included; the whiskers represent the uncertainty in the ozone tendency for plus or minus the suggested uncertainty in the rate constants. The uncertainties shown were calculated at 40°N in July for (a) 990 mbar, 100 pptv of NO_x and 30 ppbv of O_3, and (b) 190 mbar, 200 pptv of NO_x and 100 ppbv of O_3.

tion of 15 to 30% in the calculated ozone levels. Although the results presented in section 3 might be quantitatively affected by the uncertainties in the rate constants, the general conclusions reached in this section are unlikely to change.

4. Global Chemical Ozone Tendencies

The global fields of the chemical ozone tendency presented in this section are the monthly means of those calculated at every time step during an ozone simulation conducted with the Geophysical Fluid Dynamics Laboratory (GFDL) global chemistry transport model (GCTM) [*Levy et al.*, 1985; *Kasibhatla et al.*, 1996; *Levy et al.*, 1997]. NO_x and isoprene fields (isoprene is used as a proxy only) needed for this simulation are from previous GCTM runs. A detailed description of the ozone simulation and the evaluation of the results are given by *Levy at al.* [1997]. The GCTM's instantaneous chemical ozone tendencies are obtained from the tables of tendencies which were calculated with the box model with no NMHC for the zonally averaged albedo, temperature, CO, CH_4, and H_2O (as described in section 2) for four seasons (January, April, July, and October), nine latitudes (80°S, 60°S, 40°S, 20°S, equator, 20°N, 40°N, 60°N, and 80°N), seven pressure surfaces (990, 940, 835, 685, 500, 315, and 190 mbar), and a range of ozone (10, 30, 50, 70, 90, 120, 150, 250, 500 ppbv, 1, 1.5, and 2.0 ppmv), and NO_x (1, 50, 100, 200, 350, 500, 750 pptv, 1, 1.5, 2.0 ppbv) mixing ratios.

In section 3 we identified the critical parameters controlling ozone chemical tendency (NO_x, O_3, H_2O, CO, T, and solar zenith angle) and the primary sources of their variability (latitude, altitude, and season). We account for a major source of longitudinal variability in CO and albedo by constructing separate chemical tendency tables for the land and for the sea case. An example of such tendencies for the northern hemisphere over land, for just one level of ozone (50 ppbv), for one pressure surface (990 mbar) and one season (July) is depicted in Figure 8a. The instantaneous tendency in each of the GCTM's grid boxes is obtained by interpolating the values from the tables to the instantaneous values of NO_x previously computed with the same GCTM (Levy et al., manuscript in preparation, 1997), and instantaneous values of O_3 from the current simulation. Therefore, the global chemical ozone tendencies do capture the impact of the local synoptic variability in the NO_x and O_3 fields. While the calculated tendencies do not capture any variations caused by local deviations from the zonally averaged albedo, temperature, CO, CH_4, and H_2O (other than the land-sea contrast in CO and albedo), they do capture the very strong variations in these parameters due to latitude, altitude and season. The sensitivity studies from section 3 give an estimate of the error caused by using the zonally averaged parameters.

The CO/CH_4 chemical tendencies are not used in the lowest four GCTM levels (990, 940, 835, and 685 mbar) when concentration of the NMHC are likely to be high. Isoprene levels greater than 100 pptv (taken from an earlier GFDL GCTM simulation with sources from *Guenther et al.* [1995], and NO_x levels higher than 200 pptv (also taken from a previous GFDL GCTM simulation (Levy et al., manuscript in preparation, 1997)), are used as surrogate tests for elevated levels of natural and anthropogenic NMHC. In regions where either NO_x or isoprene levels imply elevated levels of NMHC, a special parameterization described by *Levy et al.* [1997] is used in the GCTM ozone simulation. In this approach the chemical ozone tendency is based on the rate of conversion of NO_x to HNO_3 with the efficiency of the conversion decreasing for higher NO_x mixing ratios [*Liu et al.*, 1987]. These parameterized chemical tendencies are excluded from the discussion below. In addition to the changes in ozone concentrations due to photochemistry, the GCTM ozone simulation contains deposition and heterogeneous removal of ozone.

4.1. Present-Day Global Chemical Ozone Tendencies

Figure 15a shows the global chemical ozone tendency fields at 990 mbar in July. White regions indicate places where either NO_x or isoprene were higher than the critical values for at least one time step during the month of July. It can be seen that the tendencies from the box model were applied generally over the oceans (where both NO_x and isoprene are low), and there they are generally small and negative. In some regions in the subtropics and tropics the chemical tendency becomes considerably more negative as a result of high solar flux and low NO_x values. Figure 15b shows the chemical tendencies at 990 mbar in January. Because of longer NO_x lifetime, in the northern hemisphere the white region occupies a greater number of grid boxes in January than in July. As in July the chemical tendencies over the ocean are generally small and negative with the belt centered on the equator being the most negative.

Figures 16a and 16b show the chemical tendency at 500 mbar for July and January. At this level the tendencies calculated with the box model were applied in all grid boxes. The tendency is highest over and downwind from the regions that have large NO_x sources. Since at 500 mbar the lightning source becomes important [*Levy et al.*, 1996], the chemical tendencies are high near the regions with high thunderstorm activity. In July there is also a large region with positive chemical tendencies in the southern hemisphere that is colocated with a plume of NO_x resulting from biomass burning in the tropics and subtropics. Over the oceans, if the grid box is not downwind from a NO_x source, there is usually destruction of ozone. In January the maxima in the chemical ozone tendency are present in different regions than in July mostly because of the change in the zenith angle, humidity, and because the distribution of NO_x changes. For example, the lightning source in the midlatitudes in the northern hemisphere disappears and so does the plume from biomass burning in the southern hemisphere.

Chemical tendencies at the next level, at 315 mbar, in July are depicted in Figure 17a. The tendencies there are generally positive (the balance point shifts to lower NO_x mixing ratios with increasing altitude), and the maximum tendencies are smaller than at 500 mbar. At this level the model shows that in July a significant fraction of NO_x in the mid and high latitudes of the northern hemisphere is of stratospheric origin, and therefore the distribution of NO_x there is more uniform (Levy et al., manuscript in preparation, 1997). There are still, however, local maxima produced by the lightning source, and the chemical ozone tendency has the highest values there. In the northern hemisphere, the slightly negative values in the high latitudes, and also midlatitudes in the winter case, are caused by high levels of ozone. At high latitudes during local winter there is no solar flux available and the chemical ozone tendencies are essentially zero.

At 190 mbar there is already little land-sea contrast in the NO_x distribution, and for this reason there is also little zonal

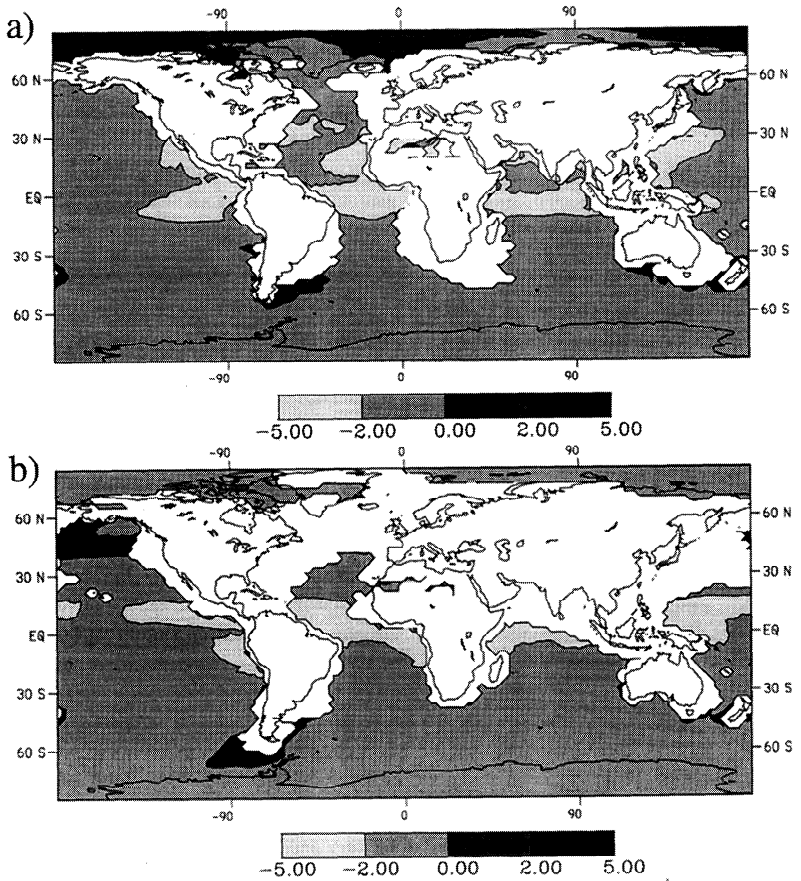

Figure 15. Monthly averaged daily chemical ozone tendency from the GCTM ozone simulation at 990 mb (a) in July and (b) in January. White places indicate regions where CO/CH_4 ozone tendencies were not used.

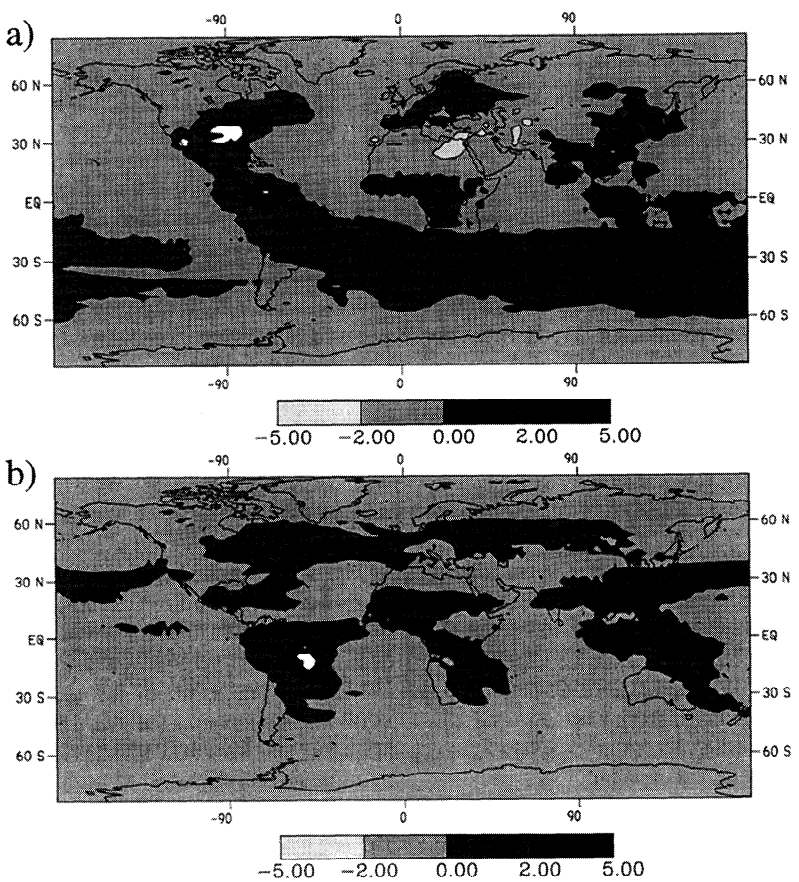

Figure 16. Monthly averaged daily chemical ozone tendency from the GCTM ozone simulation at 500 mbar (a) in July and (b) in January. White places indicate regions where ozone tendencies were above 5 ppbv/day.

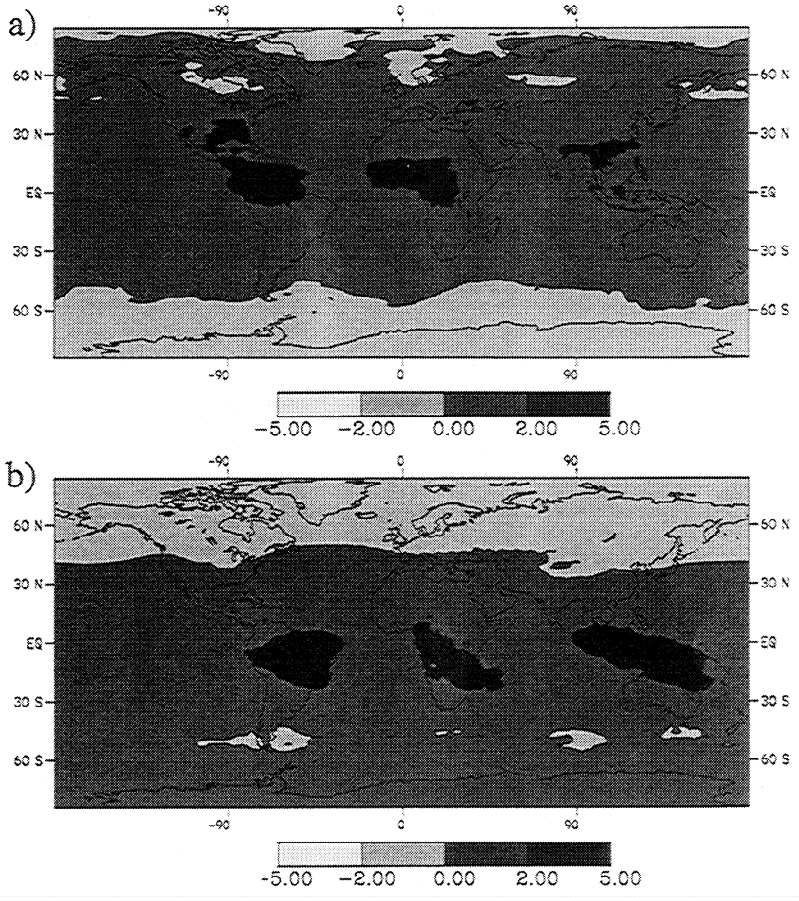

Figure 17. Monthly averaged daily chemical ozone tendency from the GCTM ozone simulation at 315 mbar (a) in July and (b) in January.

variation in the chemical ozone tendency fields (Figures 18a and 18b). The tendencies are smaller than 2 ppbv/day and generally positive. As at 315 mbar, the negative values in the high latitudes and midlatitudes of the northern hemisphere are a result of high mixing ratios of ozone, and the negative values in the winter hemispheres at high latitudes are essentially zero.

4.2. Comparison of the Daily Averaged Model Chemical Ozone Tendencies With Available Estimates From Field Campaigns

In this section an attempt is made to compare the model tendencies from this study and the tendencies estimated by *Chameides et al.* [1987] (Global Tropospheric Experiment/Chemical Instrumentation Test and Evaluation (GTE/CITE 1)), *Jacob et al.* [1992] (Atmospheric Boundary Layer Experiment (ABLE 3A)), *Liu et al.* [1992] and *Ridley et al.* [1992] (The Mauna Loa Observatory Photochemistry Experiment (MLOPEX I)), *Davis et al.* [1996] (Pacific Exploratory Mission-West (PEM-West A)), and *Jacob et al.* [1996] (Transport and Atmospheric Chemistry Near the Equator - Atlantic (TRACE A)). Only studies that estimate the diurnally averaged tendencies (and not just the tendency at the time of the measurement) for unpolluted air (low hydrocarbon concentrations) are considered. The reported estimates of the diurnally averaged ozone tendencies are based on the results from box model simulations conducted for the measured mixing ratios of the key ozone precursors. It should be emphasized here that the GCTM values as well as the estimates from field campaigns are based on current understanding of ozone's reaction mechanism. Except for MLOPEX I, the tendencies are calculated with data gathered during airplane flights, and the tendencies are the estimates given for whole basins covered by the flights. Since the tendencies can change significantly over a distance of a few hundred kilometers (Figures 15, 16, and 17) [*Chameides et al.*, 1987] and since the number of flights in each campaign is relatively small, the tendencies can only be treated as estimates of the tendencies for whole basins. The data from the campaigns and from the GCTM are compared in Table 2.

For the GTE/CITE 1 campaign the model tendencies are lower than the measured throughout the middle and lower troposphere and the switch to positive values takes place significantly higher (at around 8 km). The value for the upper troposphere agrees with the measured one. For ABLE 3A there is generally good agreement. The model value for the air at 3.4 km in the region around Hawaii is lower than the values reported by *Ridley et al.* [1992] and *Liu et al.* [1992]. Model NO_x for this region is also lower than the value reported for the MLOPEX I campaign (14 pptv in the model versus 34 pptv measured). The ozone level in the model is similar to the observed, and therefore transport of ozone is required to compensate for stronger destruction. Because the PEM-West A and TRACE-A campaigns covered both remote areas and areas affected by anthropogenic emissions and biomass

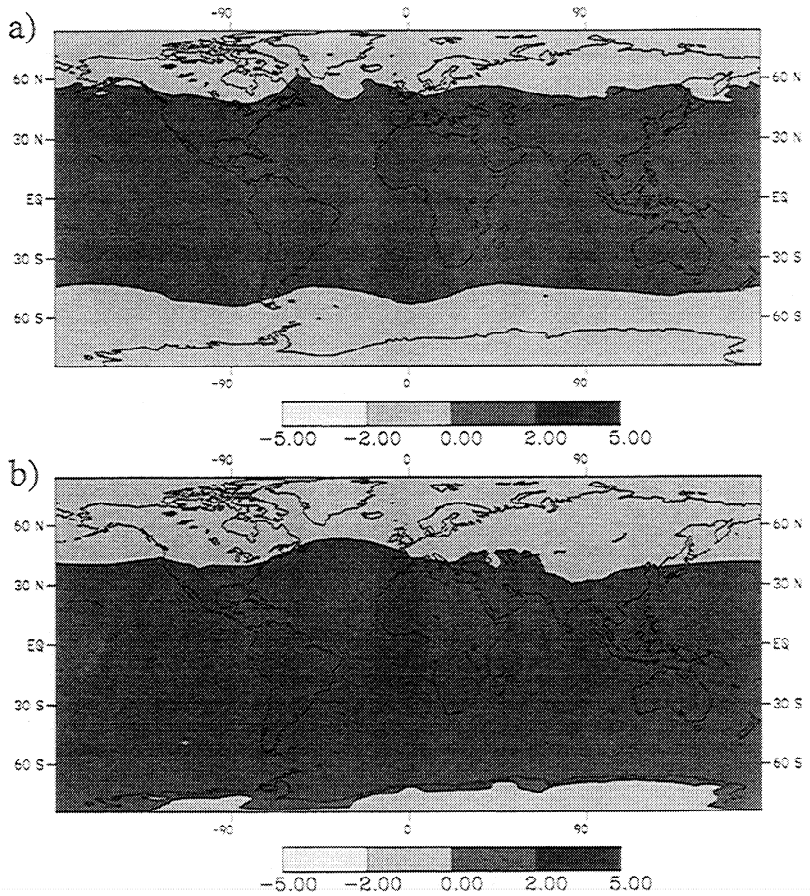

Figure 18. Monthly averaged daily chemical ozone tendency from the GCTM ozone simulation at 190 mbar (a) in July and (b) in January.

burning, the tendency changed significantly between flights. To come up with a model estimate to match the reported basin average, only the grid boxes through which the plane flew were considered. The model data are in good agreement with the PEM-West A data from 0° to 18°N, while for the data from 18°N to 42°N the model results are significantly lower. For TRACE-A the model data are higher in the middle and lower in the upper troposphere. While we capture the general altitude dependence in all cases accept GTE/CITE and have excellent quantitative agreement with ABLE 3A and PEM-West A (0-18°N), we only agree qualitatively with TRACE-A, MLOPEX I and PEM-West A (18°N-42°N). The simulated tendencies from two remote sites, Barbados and Samoa, also agree qualitatively with values estimated from the observed surface time series for these two locations [*Oltmans and Levy*, 1994].

4.3. Preindustrial Chemical Ozone Tendencies: Effect of Anthropogenic NO_x Emissions

To estimate the changes in the chemical ozone tendencies resulting from anthropogenic activities, the July global chemical ozone tendencies obtained with present-day and preindustrial NO_x fields are compared. In the preindustrial NO_x experiment the fossil fuel, aircraft, and fertilizer-induced biogenic sources of NO_x were not included, and the source from biomass burning was reduced [*Levy et al.*, 1997]. This study neglects the effect due to changes in CO and CH_4 and analyzes only the effect resulting from NO_x increases. Generally, higher NO_x in the present-day compared to preindustrial times should lead to higher chemical tendencies, but because the concentration of ozone also increases, the opposite trend can be observed in some regions (see Figures 1 and 19a). For example, at the surface, in regions over the oceans that are not significantly affected by anthropogenic NO_x sources, the chemical tendencies are generally more negative in the present-day case. This decrease is especially pronounced in the northern hemisphere where the increase in ozone is larger [*Levy et al.*, 1997]. The fact that in many regions the present chemical tendencies are lower (generally more negative) means that ozone must be transported there from other regions in order to maintain the higher, present levels of ozone.

At 500 mbar the increase in ozone caused by anthropogenic NO_x emissions is smaller than at the surface [*Levy et al.*, 1997]; therefore the chemical tendencies are less likely to decrease as a result of higher ozone fields. However, in the northern hemisphere and the tropics, with the exception of the regions over and downwind from anthropogenic NO_x sources, the increase in NO_x is still not sufficient to offset the effect of higher ozone, and the chemical tendency decreases (Figure 19b). In the southern hemisphere the increase of ozone is smaller than in the northern hemisphere, and also in July the lifetime of NO_x is longer in the southern hemisphere. These two factors are responsible for the increase of the chemical tendencies in the midlatitudes of the southern hemisphere.

Table 2. Comparison of Measured and Simulated Diurnally Averaged Chemical Ozone Tendencies

	Measured	Model
	GTE/CITE 1, (10^9molecules/cm^3/day)*	
(8<z<10km)	4.30	4.48
(4<z<8km)	4.30	-3.05
(2<z<4km)	6.90	-17.8
(0<z<2km)	-15.0	-33.0
	ABLE 3A, (ppbv/day)*	
6.5 km	-0.50	-0.36
5.5 km	-0.65	-0.57
4.5 km	-0.80	-0.68
3.5 km	-0.75	-0.79
2.5 km	-0.75	-0.54
	MLOPEX 1	
3.4 km	-0.71 [*Liu et al.*, 1992]	-1.79
3.4 km	-0.47 [*Ridley et al.*, 1992]	
	PEM WEST A, 18°N-42°N, (ppbv/day)	
10-12 km	1.44	0.68
8-10 km	1.30	0.62
6-8 km	1.00	0.32
4-6 km	-0.04	-0.31
	PEM WEST A, 0°N-18°N, (ppbv/day)	
8-10 km	0.40	0.47
6-8 km	-0.24	-0.07
4-6 km	-0.64	-0.73
2-4 km	-1.26	-1.75
	TRACE-A, (ppbv/day)	
8-12 km	2.1	1.3
4-8 km	0.3	0.9

*The measured values estimated from graph.

At 315 and at 190 mbar, because of the increased NO_x mixing ratios and only a small increase in ozone, the chemical tendencies are higher everywhere in the present case (Figures 19c and 19d), but in the preindustrial scenario they are still positive in the low latitudes and most of midlatitudes. The magnitude of the increase decreases with height being lower at 190 mbar than at 315 mbar, and lower than the maximum increase at 500 mbar. The percentage increase also generally gets smaller with altitude showing that the impact of anthropogenic NO_x emissions (which also include airplane emissions in the upper atmosphere) on the chemical ozone tendency decreases with altitude.

The globally integrated changes in the net chemical tendencies have been described by *Levy et al.* [1997] and are summarized here. The CO/CH_4 tropospheric global chemical tendency is estimated to change from a preindustrial level of -435 TgO_3/yr to a present level of -558 TgO_3/yr. The greatest change takes place in the unpolluted boundary layer where higher ozone mixing ratios are responsible for net destruction growing from -482 TgO_3/yr to -649 TgO_3/yr. In the tropical free troposphere there is a decrease in net production from +176 TgO_3/yr to +163 TgO_3/yr and in the extratropical free troposphere a decrease in destruction from -129 TgO_3/yr to -72 TgO_3/yr. The tropospheric ozone turnover time (tropospheric mass/tropospheric loss) remains essentially unchanged at ~0.2 year since the coefficient for the primary loss path, dry deposition velocity, remains unchanged and the primary chemical loss paths are not very sensitive to changes in moderate levels of NO_x.

5. Summary

The first goal of this study is to explore the dependencies of the chemical ozone tendencies on the input parameters. Our broader objective is to obtain a global perspective on the impact of the net chemical ozone tendencies on the ozone distribution.

Our study indicates that the chemical ozone tendency is especially sensitive to variations in NO_x, ozone, absolute humidity, and temperature. Decreases in absolute humidity and temperature are responsible for much lower magnitudes of the chemical tendency at higher altitudes and are also partially responsible for the significantly lower values at higher latitudes and in winter. Variations in these parameters, especially in absolute humidity, can also lead to a significant shift of the balance point and can influence the value of the NO_x mixing ratio at which the chemical ozone tendency has a maximum. The results indicate that anthropogenic changes in NO_x, CO, water vapor, and temperature can all affect the tendencies and the resulting O_3 levels and suggest possible synergisms between aircraft emissions of NO_x and CO and climate change.

The global net chemical ozone tendencies obtained from the GCTM simulation and presented in the second part of the paper show a significant decrease in the magnitudes of the chemical tendencies with height, with the maximum values at 190 mbar being smaller than 2 ppbv/day. In the upper troposphere the chemical tendencies are generally positive, while in the midtroposphere, in regions that are away from NO_x sources, the chemical tendency is generally negative. This shift to positive values with higher altitude is caused by higher NO_x mixing ratios over remote regions but also by the shift of the balance point to lower NO_x values. The maps of the global chemical ozone tendency show a close resemblance to the NO_x fields, but it has to be remembered that longitudinal variations in other parameters, particularly humidity and CO, have not been included. Currently, the only variables with longitudinal dependence are model NO_x and ozone (future studies will also include longitudinal variations of H_2O and CO). Since in the middle troposphere the NO_x sources are strongest over land regions, there is generally production of ozone over land and destruction over the oceans. In the upper troposphere this land sea contrast is generally absent. The comparisons with the estimates of the tendencies from five measurement expeditions reproduce the general profiles and sign but only show quantitative agreement with two of the five studies.

Differences between the present-day and the preindustrial chemical ozone tendencies suggest that in the boundary layer and in the midtroposphere the tendencies increased near anthropogenic NO_x sources where the increase in NO_x has a greater impact than the ozone increase. In regions away from anthropogenic sources the reverse is generally true. In the upper troposphere the tendencies increased everywhere, but the magnitude of the increase becomes smaller with increasing altitude.

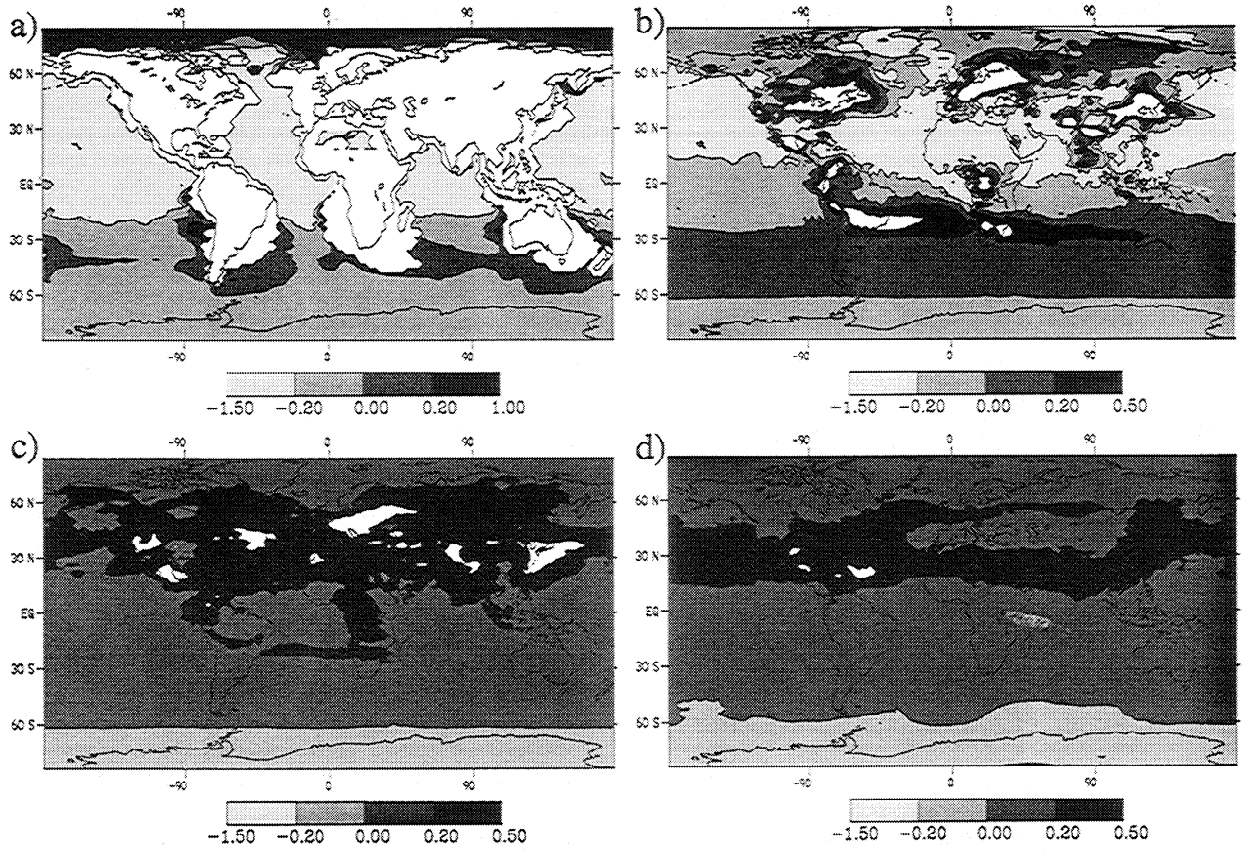

Figure 19. Difference between the monthly averaged daily chemical ozone tendencies calculated for present-day and preindustrial conditions in July at (a) 990, (b) 500, (c) 315, and (d) 190 mbar. For Figure 19a the white spaces indicate regions where CO/CH_4 ozone tendencies were not used; for Figures 19b-19d they indicate values greater than 0.5 ppbv/day.

Acknowledgments. The authors would like to thank W. Moxim and P. Kasibhatla for their assistance in carrying out this research. We would also like to thank the two anonymous reviewers as well as J. Mahlman, L. Perliski, and E. Gloor for their comments and suggestions. This research was partially supported by the NASA Earth System Science Fellowship Program, NASA Grant ESS/96-0227.

References

Barnett, J. J., and M. Corney, Temperature data from satellites, in *The Middle Atmosphere Program Handbook*, vol. 16, edited by K. Labitzke et al., pp. 3-11, 47-85, Spec. Comm. for Sol.-Terr. Phys., Secr., Univ. of Ill., Urbana, 1985.

Chameides, W. L., and J. C. G. Walker, A photochemical theory of tropospheric ozone, *J. Geophys. Res.*, *78*, 8751-8760, 1973.

Chameides, W. L., D. D. Davis, M. O. Rogers, J. Bradshaw, and S. Sandholm, Net ozone photochemical production over the eastern and central North Pacific as inferred from GTE/CITE 1 observations during fall 1983, *J. Geophys. Res.*, *92*, 2131-2152, 1987.

Chatfield, R., and H. Harrison, Ozone in the remote troposphere: Mixing versus photochemistry, *J. Geophys. Res.*, *81*, 421-423, 1976.

Climate: Long-Range Investigation, Mapping, and Prediction Project, Seasonal reconstructions of the Earth's surface at the last glacial maximum, *Geol. Soc. Am. Map Chart Ser., MC-36*, Geol. Soc. of Am., Boulder, Colo., 1981.

Crutzen, P. J., Photochemical reaction initiated by and influencing ozone in unpolluted tropospheric air, *Tellus*, *26*, 45-55, 1974.

Davis, D. D., et al., Assessment of ozone photochemistry in the western North Pacific as inferred from PEM-West A observations during the fall 1991, *J. Geophys. Res.*, *101*, 2111-2134, 1996.

DeMore, W. P., S. P. Sander, D. M. Golden, R. F. Hampson, M. J. Kurylo, C. J. Howard, A. R. Ravishankara, C. E. Kolb, and M. J. Molina, Chemical kinetics and photochemical data for use in stratospheric modeling, *JPL Publ., 94-26*, 1994.

Dentener, F. J., and P. J. Crutzen, Reaction of N_2O_5 on tropospheric aerosols: Impact on the global distributions of NO_x, O_3, and OH, *J. Geophys. Res., 98*, 7149-7163, 1993.

Fabian, P., Comments on "A photochemical theory of tropospheric ozone" by W. Chameides and J. C. G. Walker, *J. Geophys. Res., 79*, 4124-4125, 1974.

Fishman, J., and P. J. Crutzen, A numerical study of tropospheric photochemistry using a one-dimensional model, *J. Geophys. Res., 82*, 5897-5906, 1977.

Fishman, J., S. Solomon, and P. J. Crutzen, Observational and theoretical evidence in support of a significant in-situ photochemical source of tropospheric ozone, *Tellus, 31*, 432-446, 1979.

Follows, M. J., and J. F. Austin, A zonal average model of the stratospheric contributions to the tropospheric ozone budget, *J. Geophys. Res., 97*, 18,047-18,060, 1992.

Gery, M. W., G. Z. Whitten, J. P. Killus, and M. C. Dodge, A photochemical kinetics mechanism for urban and regional scale computer modeling, *J. Geophys. Res., 94*, 12,925-12,956, 1989.

Groisman, P. Y., T. R. Karl, and R. W. Knight, Changes of snow cover, temperature, and radiative heat balance over the northern hemisphere, *J. Clim., 7*, 1633-1656, 1994.

Guenther, A., et al., A global model of natural volatile organic compound emissions, *J. Geophys. Res., 100*, 8873-8892, 1995.

Hauglustaine, D. A., C. Granier, G. P. Brasseur, and G. Mégie, The importance of atmospheric chemistry in the calculations of radiative forcing on the climate system, *J. Geophys. Res., 99*, 1173-1186, 1994.

Heck, W. W., O. C. Taylor, R. Adams, G. Bingham, J. Miller, E. Preston, and L. Weinstein, Assessment of crop loss from ozone, *J. Air Pollut. Control Assoc., 32*, 818-820, 1982.

Jacob, D. J., et al., Summertime photochemistry at high northern latitudes, *J. Geophys. Res., 97*, 16,421-16,431, 1992.

Jacob, D. J., et al., Origin of ozone in the tropical troposphere: A photochemical analysis of aircraft observations over the South Atlantic basin, *J. Geophys. Res., 101*, 24,235-24,250, 1996.

Junge, C. E., Global ozone budget and exchange between stratosphere and troposphere, *Tellus, 14*, 363-377, 1962.

Kasibhatla, P. S., H. Levy II, A. A. Klonecki, and W. L. Chameides, A three-dimensional view of the large-scale tropospheric ozone distribution over the North Atlantic Ocean during summer, *J. Geophys. Res., 101*, 29,305-29,316, 1996.

Keating, G. M., M. C. Pitts, and D. F. Young, Ozone reference models for the middle atmosphere, *Adv. Space Res., 10*(12), 317-355, 1990.

Komhyr, W. D., S. J. Oltmans, P. R. Franchois, W. F. J. Evans, and W. A. Matthews, The latitudinal distribution of ozone to 35 km altitude from ECC ozonesonde observations, 1985-1987, in *Ozone in the Atmosphere*, pp. 147-150, A. Deepak Publishing, Hampton, Va., 1989.

Levy, H. II, Normal atmosphere: Large radical and formaldehyde concentrations predicted, *Science, 173*, 141-143, 1971.

Levy, H. II, J. D. Mahlman, W. J. Moxim, and S. C. Liu, Tropospheric ozone: The role of transport, *J. Geophys. Res., 90*, 3753-3772, 1985.

Levy, H. II, W. J. Moxim, and P. S. Kasibhatla, A global three-dimensional time-dependent lightning source of tropospheric NO_x, *J. Geophys. Res., 101*, 22,911-22,922, 1996.

Levy, H. II, P. S. Kasibhatla, W. J. Moxim, A. A. Klonecki, A. I. Hirsch, S. J. Oltmans, and W. L. Chameides, The human impact on global tropospheric ozone, *Geophys. Res. Lett., 24*, 791-794, 1997.

List, R., *Smithsonian Meteorological Tables*, Smithsonian Inst. Press, Washington, D. C., 1984.

Liu, S. C., D. Kley, M. McFarland, J. D. Mahlman, and H. Levy II, On the origin of tropospheric ozone, *J. Geophys. Res., 85*, 7546-7552, 1980.

Liu, S. C., M. Trainer, F. C. Fehsenfeld, D. D. Parrish, E. J. Williams, D. W. Fahey, G. Hubler, and P. C. Murphy, Ozone production in the rural troposphere and the implications for regional and global ozone distributions, *J. Geophys. Res., 92*, 4191-4207, 1987.

Liu, S. C., et al., A study of the photochemistry and ozone budgets during the Mauna Loa observatory photochemistry experiment, *J. Geophys. Res., 97*, 10,463-10,471, 1992.

Logan, J. A., Tropospheric ozone: Seasonal behavior, trends, and anthropogenic influence, *J. Geophys. Res., 90*, 10,463-10,482, 1985.

Lurmann, F. W., B. Nitta, K. Ganesan, and A. C. Lloyd, Modeling potential ozone impacts from natural sources, III, Ozone modeling in Tampa/St. Petersburg, Florida, *Atmos. Environ., 18*, 1133-1143, 1984.

Mahlman, J. D., H. Levy II, and W. J. Moxim, Three-dimensional tracer structure and behavior as simulated in the two ozone precursor experiments, *J. Atmos. Sci., 37*, 655-685, 1980.

Mauzerall, D. L., et al., Origin of tropospheric ozone at remote high northern latitudes in summer, *J. Geophys. Res., 101*, 4175-4188, 1996.

Meier, R. R., D. E. Anderson Jr., and M. Nicolet, Radiation field in the troposphere and stratosphere from 240-1000 NM, I, General analysis, *Planet. Space Sci., 30*, 923-931, 1982.

Moxim, W. J., H. Levy II, and P. S. Kasibhatla, Simulated global tropospheric PAN: Its transport and impact on NO_x, *J. Geophys. Res., 101*, 12,621-12,638, 1996.

National Research Council (NRC), *Rethinking the Ozone Problem in Urban and Regional Air Pollution*, Natl. Acad. Press, Washington, D. C., 1991.

Oltmans, S. J., and H. Levy II, Surface ozone measurements from a global network, *Atmos. Environ., 28*, 9-24, 1994.

Oort, A. H., Global atmospheric circulation statistics, 1958-1973, *NOAA Prof. Pap. 14*, 180 pp., 1983.

Orris, R. L., Ozone and temperature: A test of the consistency of models and observations in the middle atmosphere, Ph.D. thesis, Princeton Univ., Princeton, N. J., 1997.

Perliski, L. M., The role of multiple scattering in twilight zenith sky observations of atmospheric absorbers: Diurnal photochemistry and airmass factors, Ph.D. thesis, 178 pp., Univ. of Colo., Boulder, 1992.

Ramanathan, V., and R. E. Dickinson, The role of stratospheric ozone in the zonal and seasonal radiative energy balance of the Earth-tropospheric system, *J. Atmos. Sci., 36*, 1084-1104,1979.

Ridley, B. A., et al., Measurements and model simulations of the photostationary state during the Mauna Loa Observatory photochemistry experiment: Implications for radical concentrations and ozone production and loss rates, *J. Geophys. Res., 97*, 10,375-10,388, 1992.

Roelofs, G., and J. Lelieveld, Distribution and budget of O_3 in the troposphere calculated with a chemistry general circulation model, *J. Geophys. Res., 100*, 20,983-20,998, 1995.

Skarby, L., and G. Sellden, The effects of ozone on crops and forests, *Ambio, 13*, 68-72, 1984.

Spivakovsky, C. M., R. Yevich, J. A. Logan, S. C. Wofsy, and M. B. McElroy, Tropospheric OH in a three-dimensional chemical tracer model: As assessment based on observations of CH_3CCl_3, *J. Geophys. Res., 95*, 18,441-18,471, 1990.

Thompson, A. M., and R.W. Stewart, Effect of chemical kinetics uncertainties on calculated constituents in a tropospheric photochemical model, *J. Geophys. Res., 96*, 13,089-13,108, 1991.

Trainer, M., E. Y. Hsie, S. A. McKeen, R. Tallamraju, D. D. Parrish, F. C. Fehsenfeld, and S. C. Liu, Impact of natural hydrocarbons on hydroxyl and peroxy radicals at a remote site, *J. Geophys. Res., 92*, 11,879-11,894, 1987.

Trainer, M., et al., Observations and modeling of the reactive nitrogen photochemistry at a rural site, *J. Geophys. Res., 96*, 3045-3063, 1991.

Whitten, G. Z., H. Hogo, and J. P. Killus, The carbon-bond mechanism: A condensed kinetic mechanism for photochemical smog, *Environ. Sci. Technol., 14*, 690-700, 1980.

World Meteorological Organization (WMO), Scientific assessment of ozone depletion, *WMO Rep. 37*, Global Ozone Res. Monit. Proj., Geneva, 1994.

A. Klonecki, Atmospheric and Oceanic Sciences Program, Princeton University, Princeton, NJ 08540. (e-mail: aak@gfdl.gov)

H. Levy II, Geophysical Fluid Dynamics Laboratory/NOAA, P.O. Box 308, Princeton, NJ 08542. (e-mail: hl@gfdl.gov)

(Received December 20, 1996; revised May 16, 1997; accepted June 18, 1997.)